



Article

Surface Decoration of ZnWO₄ Nanorods with Cu₂O Nanoparticles to Build Heterostructure with Enhanced Photocatalysis

Lingyu Tian, Yulan Rui, Kelei Sun, Wenquan Cui and Weijia An *

College of Chemical Engineering, North China University of Science and Technology, Tangshan 063210, China; Tian165162@126.com (L.T.); tsruiyulan@163.com (Y.R.); sunkelei1986@163.com (K.S.); wkcu@163.com (W.C.)

* Correspondence: anweijia@ncst.edu.cn; Tel.: +86-151-7671-9282

Received: 1 December 2017; Accepted: 28 December 2017; Published: 9 January 2018

Abstract: The surface of ZnWO₄ nanorods was decorated with Cu₂O nanoparticles (Cu₂O/ZnWO₄) prepared through a precipitation method. The Cu₂O nanoparticles were tightly deposited on the ZnWO₄ surface and had average diameters of 20 nm. The nanoparticles not only promoted the absorption and utilization of visible light but also facilitated the separation of photogenerated charge carriers. This brought an improvement of the photocatalytic activity. The 5 wt % Cu₂O/ZnWO₄ photocatalyst displayed the highest degrade efficiency for methylene blue (MB) degradation under visible light, which was 7.8 and 2 times higher than pure ZnWO₄ and Cu₂O, respectively. Meanwhile, the Cu₂O/ZnWO₄ composite photocatalyst was able to go through phenol degradation under visible light. The results of photoluminescence (PL), photocurrent, and electrochemical impedance spectra (EIS) measurements were consistent and prove the rapid separation of charge, which originated from the match level structure and the close contact with the interface. The radical and hole trapping experiments were carried out to detect the main active substances in the photodegradation process. The holes and ·O₂⁻ radicals were predicted to dominate the photocatalytic process. Based on the characterization analysis and experiment results, a possible photocatalytic mechanism for enhancing photocatalytic activity was proposed.

Keywords: nanoparticles; ZnWO₄; degradation; photocatalysis

1. Introduction

Photocatalytic technology can directly use solar energy to degrade organic pollutants using super oxidation capacity, mild reaction conditions, and no secondary pollution. The development of an efficient semiconductor photocatalyst plays an important role in the practical application of photocatalytic technology [1]. Recently, ZnWO₄ received widespread attention due to its excellent performance in degrading organic pollutants under ultraviolet light [2,3]. Meanwhile, the ZnWO₄ photocatalyst also has the advantages of stable chemical properties and is easy to develop. However, the pure ZnWO₄ photocatalyst suffers from a higher photogenerated charge recombination rate and a low utilization rate of sunlight, which severely limits its practical application ability [4,5]. Therefore, the key problem for improving the photocatalytic performance of ZnWO₄ is to boost the rapid separation of photo-generated electron-hole pairs on the basis of efficient utilization of solar energy.

Noble metal decorated ZnWO₄ can promote the rapid separation of photogenerated charge through the schottky barrier since the Fermi level of noble metal is more positive than ZnWO₄ [5,6]. Additionally, ion doping, such as seen in fluorine and chlorine [7–10], could greatly enhance photocatalytic performance since the doped atoms can act as electron traps and promote photogenerated charge separation. In addition, construction of heterojunction photocatalyst by combining ZnWO₄ with other semiconductors, such as Bi₂WO₆/ZnWO₄ [11], ZnWO₄/BiOI [12], and BiOBr/ZnWO₄ [13], provides

a feasible route to facilitate the effective transmission of the charge through interfacial interfaces. Additionally, by combining ZnWO₄ with material that has a π - π conjugated structure like C₃N₄ [14,15] and graphene [16] could effectively inhibit the combination of photo-generated carriers due to the special conductivity of the conjugate material. Recently, Niu [17] and Li [18] prepared Ag/AgCl and Ag@AgBr nanoparticles decorate ZnWO₄ nanorods, respectively, to obtain more visible light utilization efficiency for the surface plasmon resonance of Ag nanoparticles. In addition, surface modification of ZnWO₄ with narrow band-gap and matching energy level semiconductors not only improved the visible light response but promoted the separation of the photogenerated charges.

As commonly known, Cu₂O can absorb the most visible light for the band gap at about 2.2 eV [19] when using Cu₂O nanoparticles modified for the wide bandgap semiconductor. Modifications such as TiO₂ [20], BiVO₄ [21], and BiOBr [22] can greatly enhance the absorption of visible light on the composite. Moreover, based on the morphology, the grain size of the catalyst has an important influence on the activity. Various morphologies of Cu₂O can be prepared through multiple methods [23] and exhibit excellent photocatalytic performance. Some studies have pointed out that Cu₂O nanoparticles were recently modified on the TiO₂ nanosheets or multi-walled carbon nanotubes not to enhance the light absorption but to improve the separation of the photogenerated carriers. This generates a higher photocatalytic performance [24,25]. Considering the criteria, this action loaded the Cu₂O nanoparticles onto the surface of the ZnWO₄ nanorods to further improve the utilization rate of visible light and then to stimulate production of more electron–holes. Meanwhile, the match between the level structure and the intimately contacted interface of ZnWO₄ and Cu₂O are beneficial for accelerating the separation of the photogenerated charge carriers, which improves the photocatalytic activity. In fact, there are no previous studies about using Cu₂O nanoparticles to decorate ZnWO₄ nanorods.

Herein, we modified Cu₂O nanoparticles onto the surface of ZnWO₄ nanorods. The Cu₂O nanoparticles were tightly deposited on the ZnWO₄ surface with average diameters of 20 nm. Our results proved that the Cu₂O nanoparticles greatly promoted the absorption and utilization of visible light. Meanwhile, the introduction of Cu₂O nanoparticles provides a new channel for charge transfer. This greatly inhibited photo-generated carrier recombination and accelerated the migration of interfacial charge carriers. The effects of different Cu₂O nanoparticles content on the visible light absorption and charge separation of the composites were investigated. The 5 wt % Cu₂O/ZnWO₄ photocatalyst displays the highest degrade efficiency for methylene blue (MB) degradation, which was 7.8 and 2 times more than seen in pure ZnWO₄ and Cu₂O. Based on the characterization analysis and experiment results, a possible photocatalytic mechanism on enhancement of photocatalytic activity was proposed.

2. Experimental

2.1. Synthesis of Photocatalysts

The catalyst is prepared with deionized water. The activity test process uses ultrapure water. All of the reagents are analytically graded. Initially, the synthesis of ZnWO₄ was carried out using the hydrothermal method based on previous work [26]. Typically, Na₂WO₄·2H₂O (3 mmol) and Zn(NO₃)₂·6H₂O (3 mmol) were dispersed in 25 mL distilled water with magnetic stirring for 15 min. Then, the two above aqueous solutions were mixed together through magnetic stirring at room temperature for 30 min. Afterward, the mixture was transferred into a Teflon-lined steel autoclave and the autoclaves were heated in a convection oven at 180 °C for 12 h. The resulting precipitates were collected and washed with deionized water and absolute ethanol. The samples were then dried at 80 °C for 10 h.

Then, Cu₂O/ZnWO₄ composite was prepared using a simple reductive solution chemistry route based on a previous report [22]. First, measured amounts of cetyl trimethyl ammonium bromide (CTAB) and ethylene diamine tetra acetic acid (EDTA) were dissolved in 50 mL deionized water and stirred until a stable suspension was obtained. Then, 0.5 g ZnWO₄ was added into the uniform

suspension and stirred for 30 min, followed by the addition 0.06 g $\text{Cu}(\text{Ac})_2$. Thirty minutes later, 25 mL NaOH solution ($0.45 \text{ mol}\cdot\text{L}^{-1}$) was added dropwise to the mixed solution. The color of the solution became blue, demonstrating the formation of $\text{Cu}(\text{OH})_2$. After 30 min, the solution color slowly turned to orange by adding 25 mL of ascorbic acid (AA) ($0.3 \text{ mol}\cdot\text{L}^{-1}$) solution dropwise. Finally, composites were washed with ethanol and water and dried at 60°C for 6 h to obtain $\text{Cu}_2\text{O}/\text{ZnWO}_4$.

2.2. Characterization

The crystal structure and phase analysis of the $\text{Cu}_2\text{O}/\text{ZnWO}_4$ composite was analyzed through X-ray diffraction (XRD) using a Rigaku D/MAX2500 PC diffractometer (D/MAX2500 PC, Rigaku Corporation, Tokyo, Japan) with Cu $K\alpha$ radiation, with an operating voltage of 40 kV and an operating current of 100 mA. The morphology and particle size of the catalyst were observed through transmission electron microscopy (TEM, JEM-2010, JEOL Ltd., Akishima, Japan). The UV-visible light (UV-Vis) was used to determine the light absorption properties of the catalyst (Puxi, UV1901, Beijing, China). The surface chemical state was analyzed by an X-ray photoelectron spectroscope (XPS, Shimadzu Kratos, AXIS-Ultra DLD, Tokyo, Japan) with a monochromatized Al $K\alpha$ radiation source (1486.6 eV). We performed electrochemical and photoelectrochemical measurements using a three-electrode quartz (CHI-660E, Chen Hua Instruments, Shanghai, China). Photoluminescence (PL, Hitachi F-7000, Tokyo, Japan) Spectra were collected to explore the recombination of photogenerated carriers.

2.3. Photocurrent and Electrochemical Impedance Spectra Measurements

The photocurrent and electrochemical impedance spectra (EIS) measurements were conducted using an electrochemical analyzer (CHI660E, Chen Hua Instruments, Shanghai, China) with a standard three-electrode configuration. A standard three-electrode cell was used in the photoelectric studies including a working electrode (as-prepared photocatalyst), a platinum wire as the counter electrode, and a standard calomel electrode (SCE) as the reference electrode. An amount of 0.1 M Na_2SO_4 was used as the electrolyte solution. The visible light irradiation was obtained from a 500 W Xe lamp with a 420 nm cutoff filter.

2.4. Photocatalytic Activity

The photocatalytic gradation of organic pollutants was carried out in a tube photoreactor. In order to eliminate the effect of temperature on the rate of photocatalytic degradation, the photochemical reaction apparatus was connected to a circulating cooling device (Bilon, Xi'an, China) to control the temperature of the reaction solution in the test tube at $25 \pm 2^\circ\text{C}$. The irradiation light source was a 400 W metal halide lamp. Adding the filter glass sheets between the metal halide lamp and the reaction tube filtered wavelengths $<420 \text{ nm}$. The catalyst activity was analyzed primarily by degrading 10 ppm MB by 0.1 g of catalyst. After stirring for 30 min under dark, 1 mL of sample was taken every 15 min. The collected supernatant solutions were analyzed by the spectrometer at the characteristic absorption peak of 664 nm. The samples obtained during the photocatalytic test were filtered through a filter. Additionally, the degradation of phenol solution was detected by using high performance liquid chromatography (HPLC).

3. Results and Discussion

The crystallographic structures of ZnWO_4 and $\text{Cu}_2\text{O}/\text{ZnWO}_4$ samples were confirmed by XRD measurements. As seen in Figure 1, the diffraction peaks were observed at 18.91° , 23.84° , 24.58° , 30.72° , 36.31° , 41.15° , and 53.63° , corresponding to the (110), (200), (210), (211), (220), (310), (222), (320), (321), (400) and (421) crystal surfaces of ZnWO_4 , respectively. This aligns with the standard card (JCPDS 15-0774) [27]. The standard card and the characteristic diffraction peaks were narrow and sharp, indicating that the composites possessed of high crystallinity. Meanwhile, the composites showed high purity since there were no traces of other phases examined. Compared with pure ZnWO_4 , the XRD patterns of the $\text{Cu}_2\text{O}/\text{ZnWO}_4$ composites did not vary in shapes or peaks and it was presumed that the

addition of Cu_2O did not change the crystal form of ZnWO_4 . Additionally, no characteristic diffraction peaks attributed to Cu_2O were detected in the $\text{Cu}_2\text{O}/\text{ZnWO}_4$ composites (as seen the Cu_2O JCPDS 65-3288) [22], which was caused by the small amounts and the particle size of Cu_2O nanoparticles (max 7 wt %) as well as the high dispersion of Cu_2O nanoparticles.

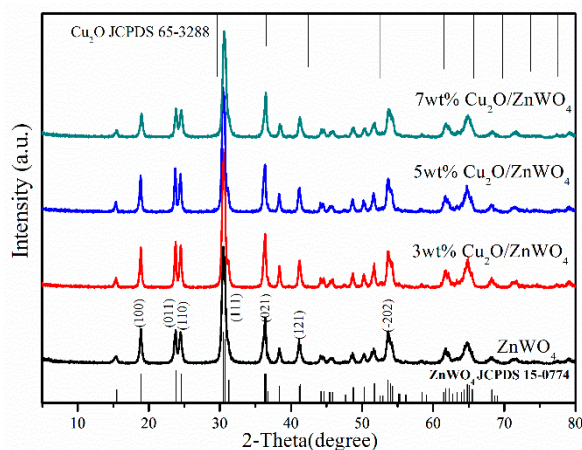


Figure 1. X-Ray Diffraction (XRD) patterns of ZnWO_4 and $\text{Cu}_2\text{O}/\text{ZnWO}_4$ photocatalysts.

The TEM was performed on the ZnWO_4 and 5 wt % $\text{Cu}_2\text{O}/\text{ZnWO}_4$ composite to investigate the morphology and detail structural information of the $\text{Cu}_2\text{O}/\text{ZnWO}_4$ composite catalyst. As seen in Figure 2a, the pure ZnWO_4 nanorods have a smooth surface with a length of 200–500 nm and a width of 20–30 nm. In comparison, as seen in Figure 2b, the Cu_2O nanoparticles, with average diameters of 20 nm, were coated on the surface of ZnWO_4 nanorods uniformly. The Cu_2O nanoparticles did not significantly change its morphology or the size of ZnWO_4 photocatalysts, which was consistent with the XRD results. Meanwhile, the Cu_2O nanoparticles were beneficial for separating the photo-generated carriers and improving the degradation performance of composites.

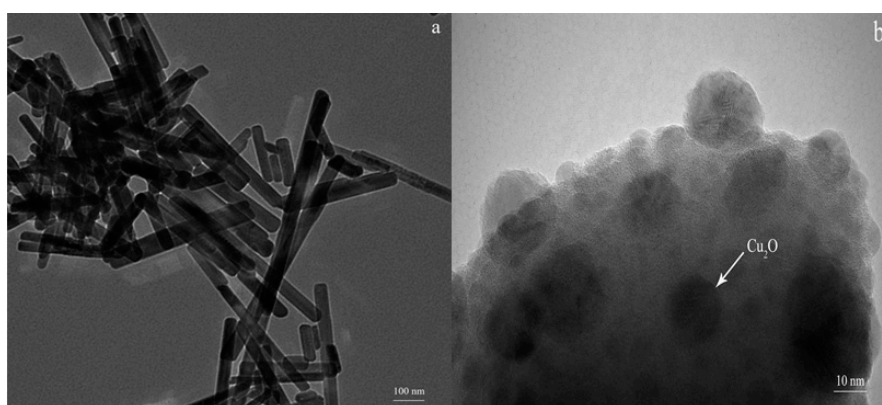


Figure 2. Transmission Electron Microscopy (TEM) images of (a) ZnWO_4 ; (b) $\text{Cu}_2\text{O}/\text{ZnWO}_4$.

Figure 3a shows the UV-visible diffuse reflectance pattern of ZnWO_4 , Cu_2O and $\text{Cu}_2\text{O}/\text{ZnWO}_4$ samples. As seen in Figure 3a, the pure ZnWO_4 shows its fundamental absorption edge at 320 nm due to its large band-gap energy while the Cu_2O exhibited strong absorption in the $\lambda < 600$ nm region. When Cu_2O nanoparticles were modified on the ZnWO_4 surface, it brought more visible light absorption for all of the $\text{Cu}_2\text{O}/\text{ZnWO}_4$ composites, and red shifted into the visible light region because of the photosensitizing effect of the incorporated Cu_2O nanoparticles. Additionally, the visible light absorption edge increased with rising Cu_2O content. The forbidden band width of a semiconductor

catalyst can be calculated using the Kubelka-Munk equation [28]. The result is shown in Figure 4b. According to the literature [21,29], the Cu_2O was a direct transition semiconductor and the ZnWO_4 was an indirect transition. As such, the band gap of pure Cu_2O and ZnWO_4 was calculated to be 1.9 and 3.7 eV (as seen in Figure 3b), respectively.

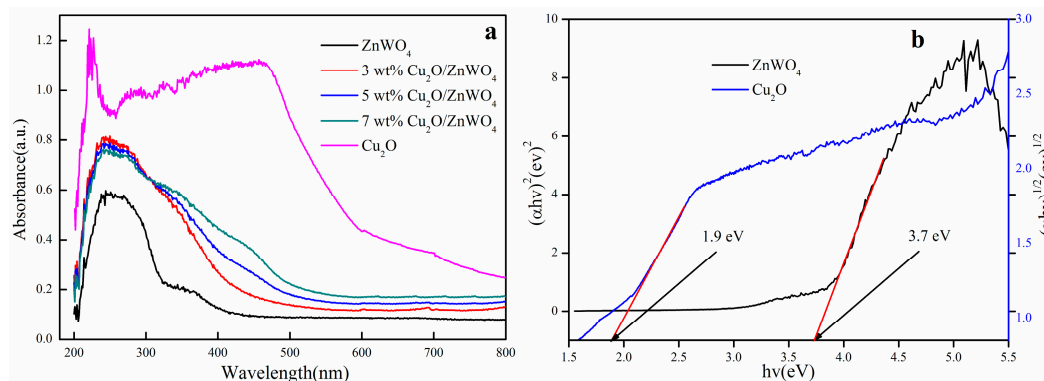


Figure 3. (a) UV-visible light (UV-vis) diffuse reflection spectra of pure ZnWO_4 , Cu_2O and $\text{Cu}_2\text{O}/\text{ZnWO}_4$ samples; (b) the band gap energies of ZnWO_4 and Cu_2O .

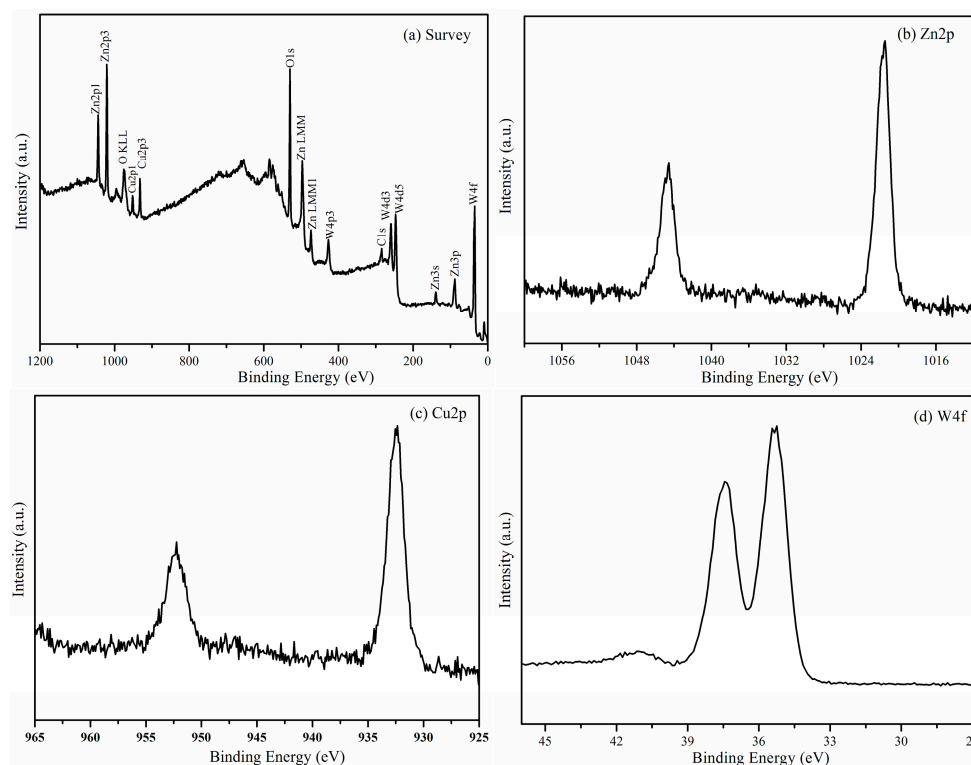


Figure 4. X-Ray Photoelectron Spectroscopy (XPS) spectra of $\text{Cu}_2\text{O}/\text{ZnWO}_4$ sample: (a) Survey of the sample; (b) Zn 2p; (c) Cu 2p and (d) W 4f.

So as to demonstrate the interaction between Cu_2O and ZnWO_4 in $\text{Cu}_2\text{O}/\text{ZnWO}_4$ composites, the valence state and the binding energy in $\text{Cu}_2\text{O}/\text{ZnWO}_4$ were determined by using XPS. The results show that the element of Cu, O, Zn, W and C all appear in the full XPS spectrum of $\text{Cu}_2\text{O}/\text{ZnWO}_4$ and the corresponding high resolution spectra, which are noted in Figure 4b–d. Zn 2p binding energy position was shown in Figure 4b. In Figure 4b, we can observe that the characteristic peaks appear at 1022.1 and 1044.5 eV, respectively, which corresponds to the peak position of $\text{Zn } 2p_{3/2}$ and

Zn 2p_{1/2} [14]. Figure 4c is the spectrum result of Cu 2p. There are two peaks shown at 931.9 and 951.9 eV, which corresponds to Cu 2p_{3/2} and Cu 2p_{1/2}, respectively. The experimental results are consistent with reports in the literature [22]. The XPS spectrum of W 4f (as seen in Figure 4d) shows that two binding energy peaks appear at 35.0 eV and at 37.4 eV, respectively for W 4f_{7/2} and W 4f_{5/2}, which determines the existence of W [30]. After the analysis of XRD and XPS, it can be concluded that Cu₂O and ZnWO₄ coexist in the Cu₂O/ZnWO₄ sample.

The photoluminescence (PL) spectra can evaluate the transfer and recombination processes of photogenerated e⁻/h⁺ pairs in semiconductors. It is widely accepted that the lower PL intensity, the lower photo-carrier recombination rate and the higher photocatalytic performance [31]. The excitation wavelength ZnWO₄ and Cu₂O in the Cu₂O/ZnWO₄ architectures was 315 nm. The comparison of PL spectra is shown in Figure 5. The main emission peak is centered at 465 nm for the ZnWO₄ sample due to the recombination of photogenerated carriers in the ZnWO₄. Once Cu₂O nanoparticles were added, the photoluminescence dropped markedly and the 5 wt % Cu₂O/ZnWO₄ composites displayed the lowest PL intensity, which indicates that the photogenerated carriers were effectively separated in the composite semiconductors. This shows that the process was conducive to promoting the photocatalytic properties of the composite material.

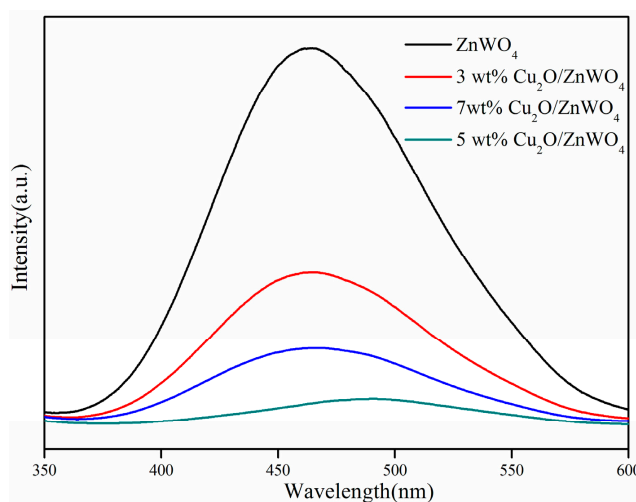


Figure 5. Photoluminescence (PL) spectra of ZnWO₄ and Cu₂O/ZnWO₄ composites.

In order to better explain the photogenerated carriers, the Cu₂O/ZnWO₄ composites should be effectively separated. The transient photocurrent responses of the ZnWO₄ and Cu₂O/ZnWO₄ composites were recorded for several on/off cycles of irradiation. It was generally considered that the higher the peak intensity, the higher the separation efficiency of the photogenerated carriers [32]. As shown in Figure 6, when visible light is irradiated, the photocurrent increases sharply. In contrast, in the dark environment, the photocurrent was immediately reduced to zero. A significant photoelectric response was observed from the on/off photoperiod. In addition, ZnWO₄ showed almost no photocurrent response due to its lack of visible light response while the Cu₂O/ZnWO₄ composites displayed much higher photocurrent intensity, where the 5 wt % Cu₂O/ZnWO₄ composites exhibited the highest photocurrent density. This shows that the introduction of Cu₂O nanoparticles will greatly improve the photocurrent response. The Cu₂O/ZnWO₄ composites exhibit faster charge separation efficiency, which originates from the ZnWO₄ and Cu₂O matching energy level structure that rapidly separates photogenerated hole pairs.

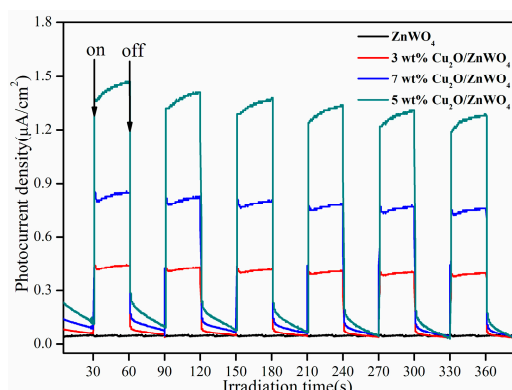


Figure 6. Photocurrent-time curves of bulk ZnWO_4 and $\text{Cu}_2\text{O}/\text{ZnWO}_4$ composites under visible light (>420 nm) irradiation with 30 s light on/off cycles.

To further test the transport rate of the electrons more intuitively, the electrochemical impedance spectra (EIS) of the prepared materials was carried out. The size of the Nyquist curve reflects the reaction rate and resistance between grain and grain, grain boundaries, and after polarization. The electrode reaction rate decreases due to a larger radius. Small arc radii imply a faster interface electron transfer for better photocatalytic ability [33]. The EIS response of ZnWO_4 and $\text{Cu}_2\text{O}/\text{ZnWO}_4$ composites in visible light irradiation is shown in Figure 7. Obviously, the semicircular diameter of the composite was smaller than pure ZnWO_4 , which demonstrates that the photo-generated charge can be effectively separated due to the strong interaction between ZnWO_4 and Cu_2O . The radius is the smallest when the composite ratio of Cu_2O is 5 wt %. All these results of EIS, photocurrent, and PL were consistent and illustrated that the introduction of Cu_2O could greatly accelerate the separation and transfer of photoelectron-hole pairs and improve the degradation performance of composites.

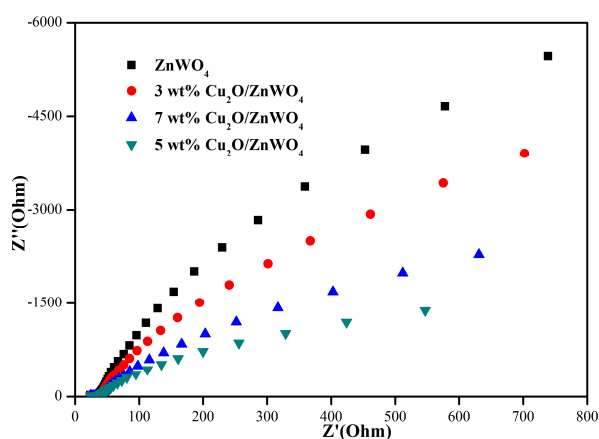


Figure 7. Electrochemical Impedance Spectra (EIS) plots of pure ZnWO_4 and as-prepared various $\text{Cu}_2\text{O}/\text{ZnWO}_4$ samples irradiated with visible light.

To determine the photocatalytic performance of the catalyst, the activity of degradation MB by ZnWO_4 , Cu_2O , and $\text{Cu}_2\text{O}/\text{ZnWO}_4$ were compared under the same experimental conditions. As seen in Figure 8a, the characteristic absorption peak of MB was 664 nm, and the intensity decreased gradually in the absence of 5 wt % $\text{Cu}_2\text{O}/\text{ZnWO}_4$ composite under visible light irradiation, and finally disappears at 90 min. Figure 8b displays the change of MB concentration (C/C_0) against photodegradation time for the prepared catalyst samples. The experimental results show that MB was not degraded in the absence of a photocatalyst or light irradiation. The MB degradation is a photocatalytic process, in which the photocatalysts generate photo-generated electron-hole pairs under illumination and further act on

the target degradation product. Pure ZnWO_4 has almost no photocatalytic activity because it does not respond to visible light. At the same time, the degradation rate of Cu_2O to MB was only 47%, which was due to the high recombination rate of excited electron-hole pairs [34]. As a comparison, the 5 wt % $\text{Cu}_2\text{O}/\text{ZnWO}_4$ composites could be degraded at about 90% MB solution, which was derived from the synergistic effect of the $\text{Cu}_2\text{O}/\text{ZnWO}_4$ composites, and achieved the rapid separation of photogenerated carriers at the heterojunction. Meanwhile, it was observed that a higher amount of Cu_2O would decrease the photocatalytic activities. At higher content, the Cu_2O nanoparticles may agglomerate and reduce the specific surface area of the composites. Additionally, extra Cu_2O particles may become the new photogenerated recombination centers and, thereby, reduce the effective photogenerated pairs. Then the particles may inhibit the composite photocatalytic performance. All these results were consistent with the PL, photocurrent, and EIS test results of the composites. Therefore, the 5 wt % $\text{Cu}_2\text{O}/\text{ZnWO}_4$ composite exhibited better photocatalytic activity.

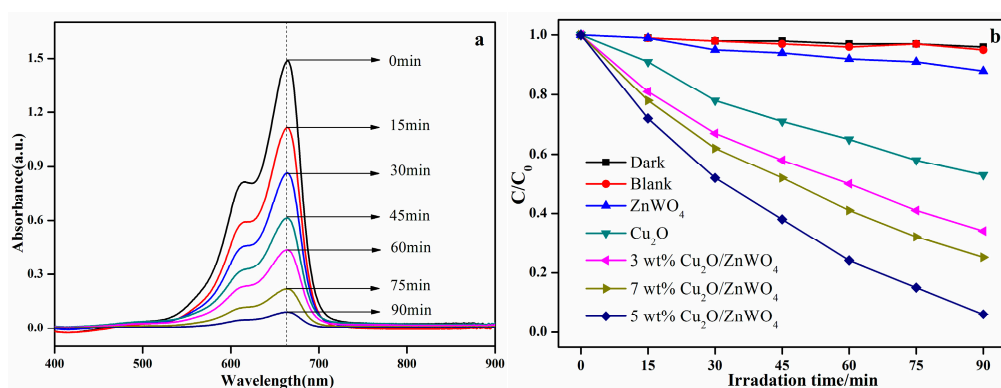


Figure 8. (a) UV-Vis spectral changes of methylene blue (MB) aqueous solution in the presence of 5 wt % $\text{Cu}_2\text{O}/\text{ZnWO}_4$ photocatalyst; (b) the activity of different catalysts to degrade MB in visible light.

Catalyst stability and reusability are also very important from the viewpoint of the catalyst's practical applications. The photocatalytic activity of the 5 wt % $\text{Cu}_2\text{O}/\text{ZnWO}_4$ composites in the degradation of MB was studied in consecutive cycles under the same conditions (as seen in Figure 9). The degradation efficiency was slightly decreased after five cycles and the final degrade rate was approximately 83%, which indicates that the Cu_2O nanoparticles modified in ZnWO_4 surface preparation of composite photocatalyst could improve the recycling performance of the catalyst and the practical application value. It could act as a potential photocatalyst for water pollution.

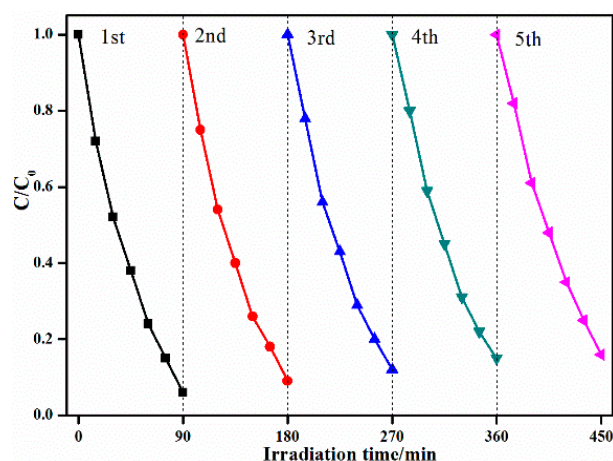


Figure 9. Stability investigation of MB photocatalytic degradation over $\text{Cu}_2\text{O}/\text{ZnWO}_4$.

In order to further study the photocatalytic degradation performance of the composites, phenol was used as the degradation object, and the same conditions were tested. It can be seen from Figure 10 that the photolysis of the phenol solution in the blank condition is negligible, and the adsorption capacity of the composite material to the phenol in the dark environment is also very limited. In contrast, the $\text{Cu}_2\text{O}/\text{ZnWO}_4$ photocatalysts exhibit higher catalytic degradation properties for phenol solution. The 5 wt % $\text{Cu}_2\text{O}/\text{ZnWO}_4$ composite photocatalyst exhibits better photocatalytic performance, which was much higher than pure Cu_2O and ZnWO_4 . This is due to the composite having a bigger advantage than Cu_2O and ZnWO_4 . More visible light responses can be excited to produce more photogenerated pairs and the photogenerated pairs can be effectively separated between the two composite interfaces, which ultimately promote the photocatalytic performance.

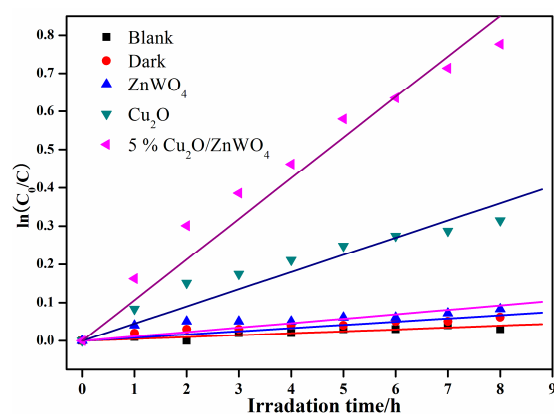


Figure 10. Linear relationship between $\ln(C_0/C)$ and light time of phenol degradation.

Quenching experiments explain the photodegradation process. In the free radical capture experiments of photodegradation, tert-butanol (TBA) and EDTA-2Na were used as capture agents for $\cdot\text{OH}$ and h^+ , respectively [30]. Meanwhile, during the course of the experiment, nitrogen was used to remove oxygen to test whether the superoxide free radicals were active species during the degradation process. As seen in Figure 11, the photodegradation efficiency was significantly suppressed when the EDTA-2Na and in the N_2 -saturated experiment condition was added, which indicates that the h^+ and O_2^- were likely the dominant active species in this process. In contrast, the dissolved $\cdot\text{OH}$ was not the main active species due to the degradation rate constant showing only a slight decline when added to the TBA solution. Therefore, the photodegradation of MB over $\text{Cu}_2\text{O}/\text{ZnWO}_4$ photocatalyst can be mainly associated with direct holes and O_2^- radicals for the photocatalytic degradation.

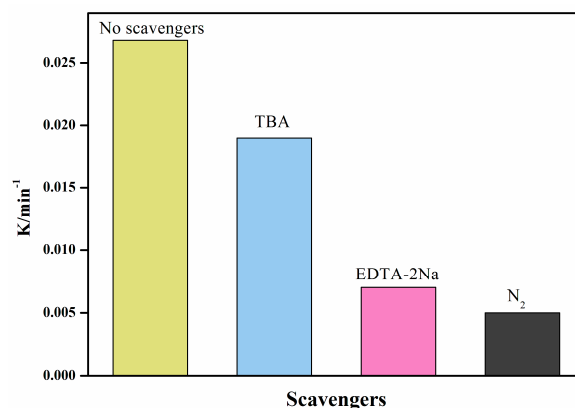


Figure 11. First-order rate constant values of photogenerated active species trapped in the system of photocatalytic degradation of MB by $\text{Cu}_2\text{O}/\text{ZnWO}_4$ under visible light.

The photocatalytic degradation kinetic curve was investigated by the first-order simplification of Langmuir-Hinshelwood (L-H) kinetics, which is well established for photocatalysis at low initial pollutant concentrations [31]. The relevant equation is as follows:

$$\ln \frac{C_0}{C} = kt$$

where C_0 and C are the concentrations of dye in solution at times 0 and t , respectively, and k is the apparent first-order rate constant (min^{-1}). The k value is obtained from the gradient of the graph of $\ln(C/C_0)$ versus time (t). Based on the characterization analysis and the experimental data, the mechanism of the high photocatalytic activities of $\text{Cu}_2\text{O}/\text{ZnWO}_4$ composites is discussed. Since the light absorption extends from ultraviolet light to visible light, there is no doubt that more visible light absorption can stimulate the generation of more photo-generated carriers, which could be effectively separated between the two composite interfaces because of the match level structure and ultimately promote the photocatalytic performance. According to the conduction band (CB) and valence band (VB) potentials of Cu_2O (-1.2 and 0.7 eV, respectively [22]) and those of ZnWO_4 (-0.8 and 2.9 eV, respectively [10]), it can be seen that $\text{Cu}_2\text{O}/\text{ZnWO}_4$ composites have matching energy levels. The staggered energy level structure contributes to the fast separation of photo-generated carriers.

The possible mechanism of improved photocatalytic performance of $\text{Cu}_2\text{O}/\text{ZnWO}_4$ composite formed by Cu_2O nanoparticles loading on ZnWO_4 was deduced based on above experimental results, as seen in Figure 12. This can be explained as follows: Under visible irradiation, Cu_2O could stimulate the generation of photogenerated hole pairs while the electrons on the conduction band can quickly migrate to the conduction band of ZnWO_4 at the close interface of the composites since the conduction band of Cu_2O is more negative than the conduction band of ZnWO_4 . Then the electrons transferred to the ZnWO_4 react with the adsorbed oxygen molecules to produce O_2^- radicals and participate in the photocatalytic oxidation degradation and the organic pollution process photocatalytic reaction. Simultaneously, after the transition stay in the Cu_2O valence band hole, another active species can directly oxidize organic pollutants involved in the reaction. Furthermore, this photo-assisted electron transfer method can effectively avoid the photo-generated carrier recombination, improve the utilization of the quantum pair, and promote the photocatalytic activity of the composite. This is consistent with the PL, photoelectric experiment results, and the active species of the quenching experiment.

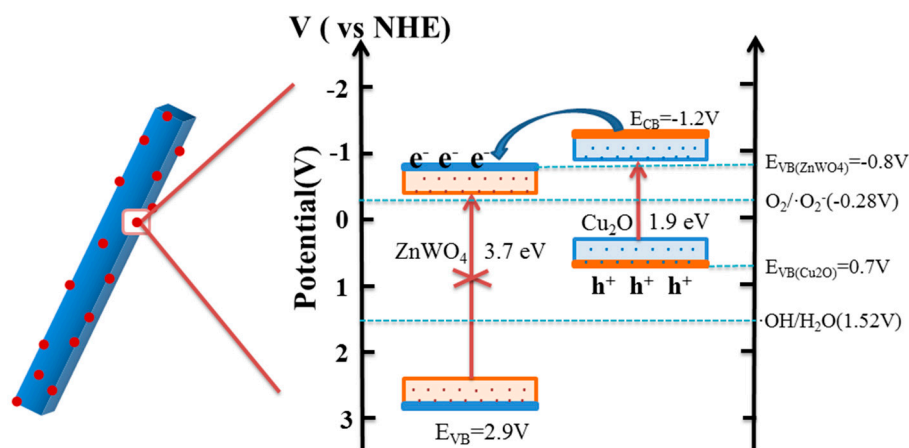


Figure 12. Schematic illustration of photo-generated carriers' transportation for $\text{Cu}_2\text{O}/\text{ZnWO}_4$ composite.

4. Conclusions

The surface of ZnWO_4 nanorods was decorated with Cu_2O nanoparticles ($\text{Cu}_2\text{O}/\text{ZnWO}_4$) prepared through the precipitation method. The 5 wt % $\text{Cu}_2\text{O}/\text{ZnWO}_4$ composites displayed the best

photocatalytic performance under visible light irradiation and the degradation rate of MB solution was 91%. The improvement in the photocatalytic performance of Cu₂O/ZnWO₄ composites due to the Cu₂O nanoparticles not only promoted the absorption and utilization of visible light, but also facilitated the migration of photogenerated charge carriers due to the matched level structure and the intimately contacted interface. In addition, the O₂⁻ and holes were predicted to be the main active species in the photocatalytic degradation process based on free-radical scavenging experiments. In conclusion, the Cu₂O/ZnWO₄ composite is a highly efficient and stable photocatalyst that can effectively degrade organic pollutants in order to protect the environment.

Acknowledgments: This work was financially supported by the National Natural Science Foundation of China (No. 51672081), Hebei Natural Science Funds for the Joint Research of Iron and Steel (B2016209348).

Author Contributions: Lingyu Tian, Yulan Rui and Weijia An conceived and designed the experiments; Lingyu Tian, Kelei Sun and Wenquan Cui analyzed the data; Lingyu Tian, Yulan Rui and Weijia An wrote the paper. All authors reviewed and approved the manuscript.

Conflicts of Interest: The authors declare no conflict of interest.

References

1. Patnaik, S.; Martha, S.; Parida, K.M. An overview of the structural, textural and morphological modulations of g-C₃N₄ towards photocatalytic hydrogen production. *RSC Adv.* **2016**, *6*, 46929–46951. [[CrossRef](#)]
2. Feng, K.L.; Huang, S.Q.; Lou, Z.Y.; Zhu, N.W.; Yuan, H.P. Enhanced photocatalytic activities of the heterostructured upconversion photocatalysts with cotton mediated on TiO₂/ZnWO₄:Yb³⁺, Tm³⁺. *Dalton Trans.* **2015**, *44*, 13681–13687. [[CrossRef](#)] [[PubMed](#)]
3. Lin, J.; Lin, J.; Zhu, Y.F. Controlled Synthesis of the ZnWO₄ Nanostructure and Effects on the Photocatalytic Performance. *Inorg. Chem.* **2007**, *46*, 8372–8378. [[CrossRef](#)] [[PubMed](#)]
4. Sun, L.M.; Zhao, X.; Cheng, X.F.; Sun, H.G.; Li, Y.L.; Li, P.; Fan, W.L. Evaluating the C, N, and F Pairwise Codoping Effect on the Enhanced Photoactivity of ZnWO₄: The Charge Compensation Mechanism in Donor Acceptor Pairs. *J. Phys. Chem. C* **2011**, *115*, 15516–15524. [[CrossRef](#)]
5. Yu, C.L.; Yu, J.C. Sonochemical fabrication, characterization and photocatalytic properties of Ag/ZnWO₄ nanorod catalyst. *Mater. Sci. Eng. B* **2009**, *164*, 16–22. [[CrossRef](#)]
6. Song, X.C.; Zheng, Y.F.; Yang, E.; Liu, G.; Zhang, Y.; Chen, H.F.; Zhang, Y.Y. Photocatalytic activities of Cd-doped ZnWO₄ nanorods prepared by a hydrothermal process. *J. Hazard. Mater.* **2010**, *179*, 1122–1127. [[CrossRef](#)] [[PubMed](#)]
7. Huang, G.L.; Zhu, Y.F. Enhanced Photocatalytic Activity of ZnWO₄ Catalyst via Fluorine Doping. *J. Phys. Chem. C* **2007**, *111*, 11952–11958. [[CrossRef](#)]
8. Huang, G.L.; Zhang, S.C.; Xu, T.G.; Zhu, Y.F. Fluorination of ZnWO₄ Photocatalyst and Influence on the Degradation Mechanism for 4-Chlorophenol. *Environ. Sci. Technol.* **2008**, *42*, 8516–8521. [[CrossRef](#)] [[PubMed](#)]
9. Chen, S.H.; Sun, S.X.; Sun, H.G.; Fan, W.L.; Zhao, X.; Sun, X. Experimental and Theoretical Studies on the Enhanced Photocatalytic Activity of ZnWO₄ Nanorods by Fluorine Doping. *J. Phys. Chem. C* **2010**, *114*, 7680–7688. [[CrossRef](#)]
10. Huang, G.L.; Zhu, Y.F. Synthesis and photoactivity enhancement of ZnWO₄ photocatalysts doped with chlorine. *CrystEngComm* **2012**, *14*, 8076–8082. [[CrossRef](#)]
11. He, D.Q.; Wang, L.L.; Xu, D.D.; Zhai, J.L.; Wang, D.J.; Xie, T.F. Investigation of Photocatalytic Activities over Bi₂WO₆/ZnWO₄ Composite under UV Light and Its Photoinduced Charge Transfer Properties. *ACS Appl. Mater. Interfaces* **2011**, *3*, 3167–3171. [[CrossRef](#)] [[PubMed](#)]
12. Li, P.; Zhao, X.; Jia, C.J.; Sun, H.G.; Sun, L.M.; Cheng, X.F.; Liu, L.; Fan, W.L. ZnWO₄/BiOI heterostructures with highly efficient visible light photocatalytic activity: the case of interface lattice and energy level match. *J. Mater. Chem. A* **2013**, *1*, 3421–3429. [[CrossRef](#)]
13. Song, X.C.; Li, W.T.; Huang, W.Z.; Zhou, H.; Zheng, Y.F.; Yin, H.Y. A novel p-n heterojunction BiOBr/ZnWO₄: Preparation and its improved visible light photocatalytic activity. *Mater. Chem. Phys.* **2015**, *160*, 251–256. [[CrossRef](#)]

14. Sun, L.M.; Zhao, X.; Jia, C.J.; Zhou, Y.X.; Cheng, X.F.; Li, P.; Liu, L.; Fan, W.L. Enhanced visible-light photocatalytic activity of g-C₃N₄-ZnWO₄ by fabricating a heterojunction: investigation based on experimental and theoretical studies. *J. Mater. Chem.* **2012**, *22*, 23428–23438. [[CrossRef](#)]
15. Wang, Y.J.; Wang, Z.X.; Muhammad, S.; He, J. Graphite-like C₃N₄ hybridized ZnWO₄ nanorods: Synthesis and its enhanced photocatalysis in visible light. *CrystEngComm* **2012**, *14*, 5065–5070. [[CrossRef](#)]
16. Bai, X.J.; Wang, L.; Zhu, Y.F. Visible Photocatalytic Activity Enhancement of ZnWO₄ by Graphene Hybridization. *ACS Catal.* **2012**, *2*, 2769–2778. [[CrossRef](#)]
17. Ke, J.; Niu, C.G.; Zhang, J.; Zeng, G.M. Significantly enhanced visible light photocatalytic activity and surface plasmon resonance mechanism of Ag/AgCl/ZnWO₄ composite. *J. Mol. Catal. A Chem.* **2014**, *395*, 276–282. [[CrossRef](#)]
18. Li, K.B.; Xue, J.; Zhang, Y.H.; Wei, H.; Liu, Y.L.; Dong, C.X. ZnWO₄ nanorods decorated with Ag/AgBr nanoparticles as highly efficient visible-light-responsive photocatalyst for dye AR18 photodegradation. *Appl. Surf. Sci.* **2014**, *320*, 1–9. [[CrossRef](#)]
19. Zhang, Z.H.; Du, R.; Zhang, L.B.; Zhu, H.B.; Zhang, H.N.; Wang, P. Carbon-Layer-Protected Cuprous Oxide Nanowire Arrays for Efficient Water Reduction. *ACS Nano* **2013**, *7*, 1709–1717. [[CrossRef](#)] [[PubMed](#)]
20. Wang, M.Y.; Sun, L.; Lin, Z.Q.; Cai, J.H.; Xie, K.P.; Lin, C.J. P-N heterojunction photoelectrodes composed of Cu₂O-loaded TiO₂ nanotube arrays with enhanced photoelectrochemical and photoelectrocatalytic activities. *Energy Environ. Sci.* **2013**, *6*, 1211–1220. [[CrossRef](#)]
21. Wang, W.Z.; Huang, X.W.; Wu, S.; Zhou, Y.X.; Wang, L.J.; Shi, H.L.; Liang, Y.J.; Zou, B. Preparation of p-n junction Cu₂O/BiVO₄ heterogeneous nanostructures with enhanced visible-light photocatalytic activity. *Appl. Catal. B* **2013**, *134–135*, 293–301. [[CrossRef](#)]
22. Cui, W.Q.; An, W.J.; Liu, L.; Hu, J.S.; Liang, Y.H. Novel Cu₂O quantum dots coupled flower-like BiOBr for enhanced photocatalytic degradation of organic contaminant. *J. Hazard. Mater.* **2014**, *280*, 417–427. [[CrossRef](#)] [[PubMed](#)]
23. Zhang, Z.L.; Che, H.W.; Wang, Y.L.; Gao, J.J.; Zhao, L.R.; She, X.L.; Sun, J.; Poernomo, G.W.; Zhong, Z.Y.; Su, F.B. Facile Synthesis of Mesoporous Cu₂O Microspheres with Improved Catalytic Property for Dimethyldichlorosilane Synthesis. *Ind. Eng. Chem. Res.* **2012**, *51*, 1264–1274. [[CrossRef](#)]
24. Liu, L.C.; Gu, X.R.; Sun, C.Z.; Li, H.; Deng, Y.; Gao, F.; Dong, L. In situ loading of ultra-small Cu₂O particles on TiO₂ nanosheets to enhance the visible-light photoactivity. *Nanoscale* **2012**, *4*, 6351–6359. [[CrossRef](#)] [[PubMed](#)]
25. Song, S.Q.; Rao, R.C.; Yang, H.X.; Zhang, A.M. Cu₂O/MWCNTs Prepared by Spontaneous Redox: Growth Mechanism and Superior Catalytic Activity. *J. Phys. Chem. C* **2010**, *114*, 13998–14003. [[CrossRef](#)]
26. Yu, S.H.; Liu, B.; Mo, M.S.; Huang, J.H.; Liu, X.M.; Qian, Y.T. General synthesis of single-crystal tungstate nanorods/nanowires: A facile, low-temperature solution approach. *Adv. Funct. Mater.* **2003**, *13*, 639–647. [[CrossRef](#)]
27. Hojamberdieva, M.; Katsumata, K.; Morita, K.; Bilmes, S.A.; Matsushita, N.; Okada, K. One-step hydrothermal synthesis and photocatalytic performance of ZnWO₄/Bi₂WO₆ composite photocatalysts for efficient degradation of acetaldehyde under UV light irradiation. *Appl. Catal. A Gen.* **2013**, *457*, 12–20. [[CrossRef](#)]
28. Chen, Z.H.; Bing, F.; Liu, Q.; Zhang, Z.G.; Fang, X.M. Novel Z-scheme visible-light-driven Ag₃PO₄/Ag/SiC photocatalysts with enhanced photocatalytic activity. *J. Mater. Chem. A* **2015**, *3*, 4652–4658. [[CrossRef](#)]
29. Khyzhuna, O.Y.; Bekeneva, V.L.; Atuchinb, V.V.; Galashovc, E.N.; Shlegelc, V.N. Electronic properties of ZnWO₄ based on ab initio FP-LAPW band-structure calculations and X-ray spectroscopy data. *Mater. Chem. Phys.* **2013**, *140*, 588–595. [[CrossRef](#)]
30. Hu, J.S.; An, W.J.; Wang, H.; Geng, J.P.; Cui, W.Q.; Zhan, Y. Synthesis of a hierarchical BiOBr nanodots/Bi₂WO₆ p-n heterostructure with enhanced photoinduced electric and photocatalytic degradation performance. *RSC Adv.* **2016**, *6*, 29554–29562. [[CrossRef](#)]
31. An, W.J.; Cui, W.Q.; Liang, Y.H.; Hu, J.S.; Liu, L. Surface decoration of BiPO₄ with BiOBr nanoflakes to build heterostructure photocatalysts with enhanced photocatalytic activity. *Appl. Surf. Sci.* **2015**, *351*, 1131–1139. [[CrossRef](#)]
32. Liu, L.; Ding, L.; Liu, Y.G.; An, W.J.; Lin, S.L.; Liang, Y.H.; Cui, W.Q. A stable Ag₃PO₄@PANI core@shell hybrid: Enrichment photocatalytic degradation with π-π conjugation. *Appl. Catal. B* **2017**, *201*, 92–104. [[CrossRef](#)]

33. Chen, F.Y.; An, W.J.; Liu, L.; Liang, Y.H.; Cui, W.Q. Highly efficient removal of bisphenol A by a three-dimensional graphene hydrogel-AgBr@rGO exhibiting adsorption/photocatalysis synergy. *Appl. Catal. B* **2017**, *217*, 65–80. [[CrossRef](#)]
34. Ai, Z.H.; Xiao, H.Y.; Mei, T.; Liu, J.; Zhang, L.Z.; Deng, K.J.; Qiu, J.R. Electro-fenton degradation of Rhodamine B based on a composite cathode of Cu₂O nanocubes and carbon nanotubes. *J. Phys. Chem. C* **2008**, *112*, 11929–11935. [[CrossRef](#)]



© 2018 by the authors. Licensee MDPI, Basel, Switzerland. This article is an open access article distributed under the terms and conditions of the Creative Commons Attribution (CC BY) license (<http://creativecommons.org/licenses/by/4.0/>).